AMERICAN SOCIETY FOR MICROBIOLOGY | Infection and Immunity®

CELLULAR MICROBIOLOGY:
PATHOGEN-HOST CELL MOLECULAR INTERACTIONS

# The Enterohemorrhagic *Escherichia coli* Effector EspW Triggers Actin Remodeling in a Rac1-Dependent Manner

**Pamela Sandu,[a] Valerie F. Crepin,[a] Hauke Drechsler,[b] Andrew D. McAinsh,[b] Gad Frankel,[a] Cedric N. Berger[a]**

MRC Centre for Molecular Bacteriology and Infection, Department of Life Sciences, Imperial College London, London, United Kingdom[a]; Centre for Mechanochemical Cell Biology, Division of Biomedical Cell Biology, Warwick Medical School, University of Warwick, Coventry, United Kingdom[b]

**ABSTRACT** Enterohemorrhagic *Escherichia coli* (EHEC) is a diarrheagenic pathogen that colonizes the gut mucosa and induces attaching-and-effacing lesions. EHEC employs a type III secretion system (T3SS) to translocate 50 effector proteins that hijack and manipulate host cell signaling pathways, which allow bacterial colonization and subversion of immune responses and disease progression. The aim of this study was to characterize the T3SS effector EspW. We found *espW* in the sequenced O157:H7 and non-O157 EHEC strains as well as in *Shigella boydii*. Furthermore, a truncated version of EspW, containing the first 206 residues, is present in EPEC strains belonging to serotype O55:H7. Screening a collection of clinical EPEC isolates revealed that *espW* is present in 52% of the tested strains. We report that EspW modulates actin dynamics in a Rac1-dependent manner. Ectopic expression of EspW results in formation of unique membrane protrusions. Infection of Swiss cells with an EHEC *espW* deletion mutant induces a cell shrinkage phenotype that could be rescued by Rac1 activation via expression of the bacterial guanine nucleotide exchange factor, EspT. Furthermore, using a yeast two-hybrid screen, we identified the motor protein Kif15 as a potential interacting partner of EspW. Kif15 and EspW colocalized in cotransfected cells, while ectopically expressed Kif15 localized to the actin pedestals following EHEC infection. The data suggest that Kif15 recruits EspW to the site of bacterial attachment, which in turn activates Rac1, resulting in modifications of the actin cytoskeleton that are essential to maintain cell shape during infection.

**KEYWORDS** EHEC, EPEC, Kif15, Rac1, Rho GTPase, actin, *espW*

The human pathogens enterohemorrhagic *Escherichia coli* (EHEC) and enteropathogenic *E. coli* (EPEC) (1) and the mouse pathogen *Citrobacter rodentium* (CR) (2) constitute a bacterial family that colonizes the intestinal mucosa and induces the formation of attaching-and-effacing (A/E) lesions. The A/E lesions are characterized by effacement of the brush border microvilli, intimate attachment of the bacteria to the apical membrane of host epithelial cells, and induction of actin polymerization beneath the attached bacteria (3). EPEC, EHEC, and *C. rodentium* employ a filamentous type III secretion system (T3SS) (4), located within the locus of enterocyte effacement (LEE) (5), to translocate a plethora of effector proteins directly from the bacterial cell into host cell cytoplasm (6). Of the translocated effectors, five (Tir, EspZ, EspH, EspG, and Map) are LEE encoded. The effector Tir plays a key role in formation of A/E lesions *in vivo* (7) and in actin-rich pedestals in cultured cells (8). Following clustering by the LEE-encoded outer membrane adhesin intimin, EPEC Tir ($Tir_{EPEC}$) and *C. rodentium* Tir ($Tir_{CR}$) bind Nck, while EHEC Tir ($Tir_{EHEC}$) binds the adaptor proteins IRTKS and/or IRSp53 (9, 10) and recruits the effector TccP/EspFu (11, 12). The Tir signaling pathways then converge on N-WASP and the ARP2/3 complex, leading to actin polymerization (13).

**Received** 4 April 2017 **Returned for modification** 10 May 2017 **Accepted** 14 June 2017

**Accepted manuscript posted online** 19 June 2017

**Citation** Sandu P, Crepin VF, Drechsler H, McAinsh AD, Frankel G, Berger CN. 2017. The enterohemorrhagic *Escherichia coli* effector EspW triggers actin remodeling in a Rac1-dependent manner. Infect Immun 85:e00244-17. https://doi.org/10.1128/IAI.00244-17.

**Editor** Shelley M. Payne, University of Texas at Austin



Address correspondence to Cedric N. Berger, c.berger@imperial.ac.uk.

The actin cytoskeleton, which is targeted by many bacterial pathogens, is essential for cell integrity, motility, membrane trafficking, and shape changes (14). Rho GTPases, which belong to the family of Ras-related small GTPases, are key regulators of various cellular processes, including actin polymerization, microtubule dynamics, vesicle trafficking, cell polarity, and cytokinesis (15). The best-characterized members of the Rho GTPase family are RhoA, Rac1, and Cdc42, the activation of which leads to the assembly of stress fibers, lamellipodia/ruffles, and filopodia, respectively (16). Switching of Rho GTPases from an inactive GDP-bound state to an active GTP-bound state is mediated by guanine nucleotide exchange factors (GEFs). The switch back from the active GTP to an inactive GDP-bound state is regulated by GTPase-activating proteins (GAPs). In their GTP-bound conformation, Rho GTPases interact with and activate downstream target effectors, such as serine/threonine kinases, tyrosine kinases, lipid kinases, lipases, oxidases, and scaffold proteins (17). As Rho GTPases are important regulators of the actin cytoskeleton, bacterial pathogens have evolved strategies to subvert their signaling during infection.

Bacterial guanine nucleotide exchange factors, which belong to the SopE family, act as bacterial Rho GEFs to activate the host Rho GTPase (18). The A/E pathogen effector Map induces filopodia via Cdc42 at the site of attachment (19, 20), EspM promotes stress fibers via RhoA activation (21), and EspT triggers ruffle and lamellipodia formation by Rac1 (22). A/E pathogens also translocate effectors that inactivate Rho GTPases. EspH globally inactivates DH-PH domain mammalian Rho-GEFs but not the bacterial Rho-GEFs (23). Tir antagonizes the activity of Map as it downregulates formation of filopodia (24), while EspO2 interacts with EspM2 and blocks formation of the stress fibers (25).

Using a transfection-based screen, we recently identified $EspW_{EHEC}$ as a regulator of actin filament organization. EspW has been shown previously to be secreted by EHEC and translocated into mammalian cells in a type 3-dependent manner (26). However, until now, no function has been identified for this effector. The aim of this study was to investigate the role of EspW during EHEC infection and its putative role as a Rho GTPase regulator.

## RESULTS

**Screening of *espW* in EPEC clinical isolates.** EspW is a 352-amino-acid effector and is located in the SP17 pathogenic island, which also encodes EspM2 and members of the NleG family (see Fig. S1A in the supplemental material). So far, EspW has been reported only in EHEC O157:H7 and EPEC B171 (O111:H$^-$) strains, with no homologs among other bacterial species. Using the BLAST algorithm with EspW as the index protein, we confirmed that it was present in the sequenced EHEC O157:H7 strains, in five non-O157:H7 EHEC strains (O111:H$^-$, O111:H11, O26:H11, O103:H2, and O103:H25), and in *Shigella boydii* (Fig. S1B). Furthermore, a putative coding sequence for a truncated version of EspW containing the N-terminal 206 amino acids ($EspW_{1–206}$) was present in two EPEC strains (CB9615 and RM12579) belonging to serotype O55:H7 (Fig. S2), a progenitor of EHEC O157:H7 (27). In order to determine if either the long or short versions of *espW* are present in other EPEC strains, we screened by PCR a collection of 132 clinical isolates available in our laboratory. This revealed that the long version of *espW* is present in 52% of the tested stains (Table 1). Furthermore, $espW_{1–206}$ was found in 10 of the 132 (8%) strains tested (Table 1). Interestingly, 9 of the 10 $espW_{1–206}$ genes belonged to serotype O55:H7. Neither of the *espW* variants was found in *C. rodentium* and the prototype EPEC strain E2348/69, while the prototype atypical EPEC strain E110019 (O111:H9) contains the long version of *espW*.

**EspW interacts with the C terminus of Kif15.** In order to identify the EspW host cell partner protein, we performed a yeast two-hybrid screen using a HeLa cell cDNA library as bait and identified the carboxy terminus of Kif15, $Kif15_{1092–1368}$, as a putative partner. The interaction was confirmed by direct yeast two-hybrid (DY2H). Importantly, $Kif15_{1092–1368}$ interacted with the full-length EspW (Fig. 1B) but not with $EspW_{1–206}$. To further map the binding site of EspW to Kif15, five Kif15 truncation fragments were generated and tested by DY2H (Fig. 1A). An empty pGAD-T7 plasmid was used as a

**TABLE 1** Distribution of *espW* and $espW_{1–206}$ among 132 clinical EPEC isolates[a]

| Serogroup (no. of strains) | No. of strains carrying *espW* | Serotype (no. of strains/total no. of strains tested) |
|---|---|---|
| ONT (3) | 3 | H7 (1/1); H45 (1/1); $H^-$ (1/1) |
| O13 (1) | 1 | $H^-$ (1/1) |
| O26 (13) | 9 | $H^-$ (4/8); H11 (5/5) |
| O49 (1) | 1 | $H^-$ (1/1) |
| O55 (24) | 10 | $H^-$ (3/11); H6 (5/5); H7 (1/5); H34 (1/3) |
| O86 (5) | 3 | H8 (0/2); H34 (3/3) |
| O104 (1) | 1 | H2 (1/1) |
| O109 (1) | 1 | H9 (1/1) |
| O111 (12) | 5 | $H^-$ (2/4); H2 (3/3); H9 (0/1); H12 (0/1); H21 (0/1); H25 (0/2) |
| O114 (3) | 2 | $H^-$ (0/1); H2 (2/2) |
| O119 (29) | 14 | H2 (4/11); H4 (0/1); H6 (10/17) |
| O123 (1) | 1 | $H^-$ (1/1) |
| O125 (3) | 1 | H6 (1/3) |
| O126 (4) | 1 | $H^-$ (1/1); H27 (0/3) |
| O127 (8) | 3 | $H^-$ (1/1); H6 (2/3); H27 (0/1); H40 (0/3) |
| O128 (6) | 4 | $H^-$ (0/1); H2 (4/4); H35 (0/1) |
| O142 (7) | 5 | H6 (3/3); H34 (2/4) |
| O153 (1) | 1 | $H^-$ (1/1) |
| O154 (1) | 1 | H9 (1/1) |
| O177 (1) | 1 | H11 (1/1) |

[a]*espW* was present in 68 out of 132 EPEC strains screened; 10 out of the 64 PCR-negative strains (O26:$H^-$ [1 strain], O55:$H^-$ [5 strains], and O55:H7 [4 strains]) were $espW_{1–206}$ positive. The following strains were *espW* and $espW_{1–206}$ negative: O2:H49 (1 strain), O6:H19 (2 strains), O45:$H^-$ (1 strain), O85:$H^-$ (1 strain), and O118:H5 (2 strains).

negative control. No growth was observed on selected media (QDO) when yeast were cotransformed with EspW and $Kif15_{1142–1347}$, $Kif15_{1142–1368}$, or the negative control. In contrast, growth was seen following cotransformation with EspW and $Kif15_{1092–1347}$ or $Kif15_{1092–1142}$ (Fig. 1C), suggesting that the C-terminus coil-coil domain of Kif15 plays an important role in the interaction with EspW.

**Kif15 localizes to the pedestals and colocalizes with EspW.** We aimed to determine the localization of Kif15 during EHEC infection. However, we were unable to detect endogenous Kif15, and localization of overexpressed Kif15 was difficult to detect due to poor transfection efficiency. Accordingly, we determined the localization of ectopically expressed $Kif15_{1092–1368}$, used in the DY2H, following EHEC infection of transfected Swiss 3T3 cells. Cells expressing myc-green fluorescent protein (GFP) were used as a negative control. Immunofluorescence (IF) microscopy revealed that $Kif15_{1092–1368}$, but not GFP, localized to the actin pedestals at the site of EHEC attachment (Fig. 1D). Interestingly, cells transfected with $Kif15_{1092–1368}$ and infected with an EHEC Δ*espW* strain present a similar recruitment of $Kif15_{1092–1368}$ into the pedestal (Fig. S3), suggesting EspW is not required for localization of Kif15 to the pedestal.

We next aimed to determine if $Kif15_{1092–1368}$ and EspW colocalized. For this, we first tried to hemagglutinin (HA) tag EspW in EHEC; however, no signal could be detected by IF. Therefore, we cotransfected cells with pRK5-HA-*espW* and pRK5-Myc-$kif15_{1092–1368}$. pRK5-HA-*mCherry* served as a negative control. EspW and $Kif15_{1092–1368}$ colocalized, whereas no colocalization was observed between mCherry and $Kif15_{1092–1368}$ (Fig. 1E). Interestingly, EspW and $Kif15_{1092–1368}$ were also present at membrane sites showing actin reorganization.

**EspW triggers actin remodelling in a Rac1-dependent manner.** In order to determine if EspW is responsible for the observed actin reorganization (Fig. 1E), we transfected cells with pRK5-HA-*espW*, pRK5-HA-$espW_{1–206}$, or pRK5 encoding GFP as a negative control. Immunofluorescence staining (Fig. 2A) and scanning electron microscopy (SEM) (Fig. 2B) revealed that the full-length EspW triggered formation of either membrane ruffles (13% of transfected cells) or flower-shaped structures (42% of transfected cells), which were rich in actin and colocalized with EspW (Fig. 2A to C).

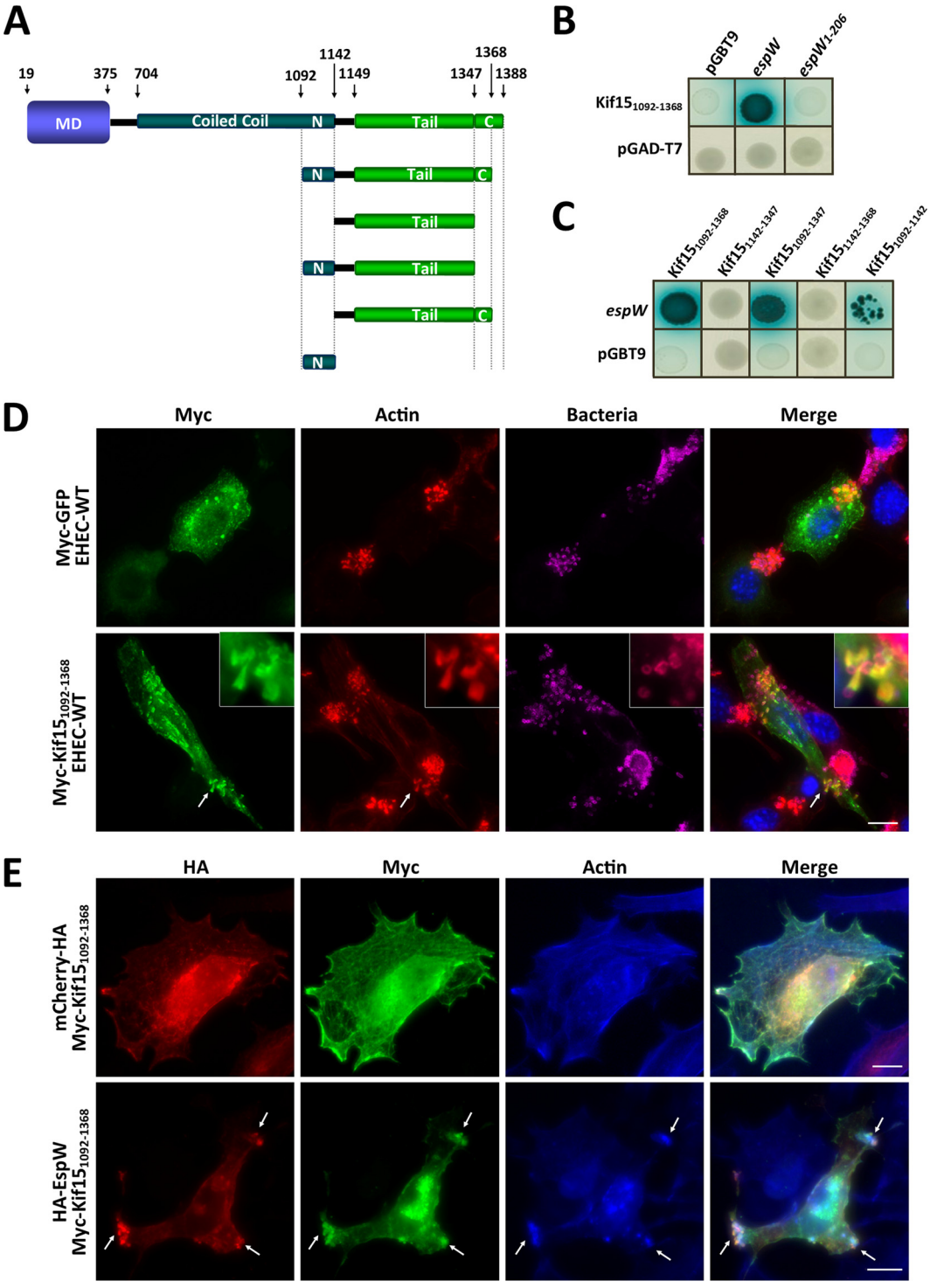


**FIG 1** Kif15 interacts with EspW. (A) Schematic representation of Kif15. (B) Direct yeast two-hybrid assay revealed that EspW, but not $EspW_{1-206}$, interacts with $Kif15_{1092-1368}$. (C) EspW interacts with $Kif15_{1092-1368}$, $Kif15_{1092-1347}$, and $Kif15_{1092-1142}$, but not $Kif15_{1142-1368}$ and $Kif15_{1142-1347}$, by direct yeast two-hybrid assay. (D) Following infection of transfected $Kif15_{1092-1368}$ (green) cells, $Kif15_{1092-1368}$ localized at the actin (red) pedestals (white arrows), under adherent EHEC (magenta). DNA was visualized by Hoechst staining (blue). (E) Ectopically expressed $Kif15_{1092-1368}$ (green) colocalized with EspW (red) and actin (magenta), but not mCherry, in Swiss 3T3 cells. Bar, 10 $\mu$m.

$EspW_{1-206}$ showed aggregative localization dispersed within the cell with an actin structure similar to those seen in the GFP control cells (Fig. 2A and B).

In order to determine if EspW-induced actin remodelling requires RhoA, Rac-1, or Cdc42, we cotransfected HeLa cells with pRK5-HA-*espW* and a dominant negative of

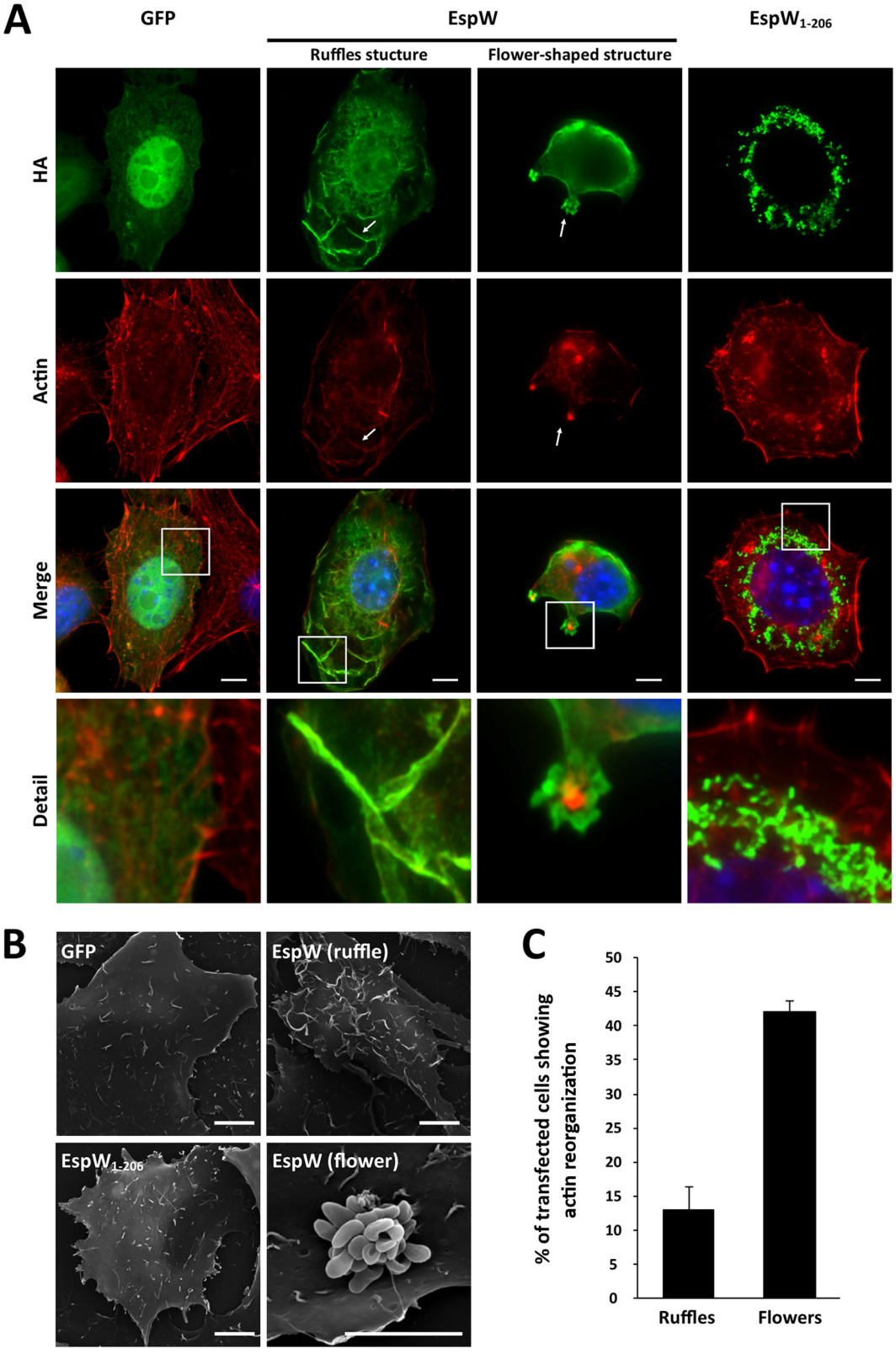


**FIG 2** EspW induces actin rearrangement. (A) Ectopic expression of HA-EspW (green) induces either actin (red) ruffles or flower-shaped structures. No actin modification can be observed with HA-EspW$_{1–206}$ or GFP (green). DNA was visualized by Hoechst staining (blue). White arrows indicate colocalization of EspW with actin. Bar, 5 $\mu$m. (B) SEM of transfected cells. (C) Quantification of actin structure observed in transfected cells.

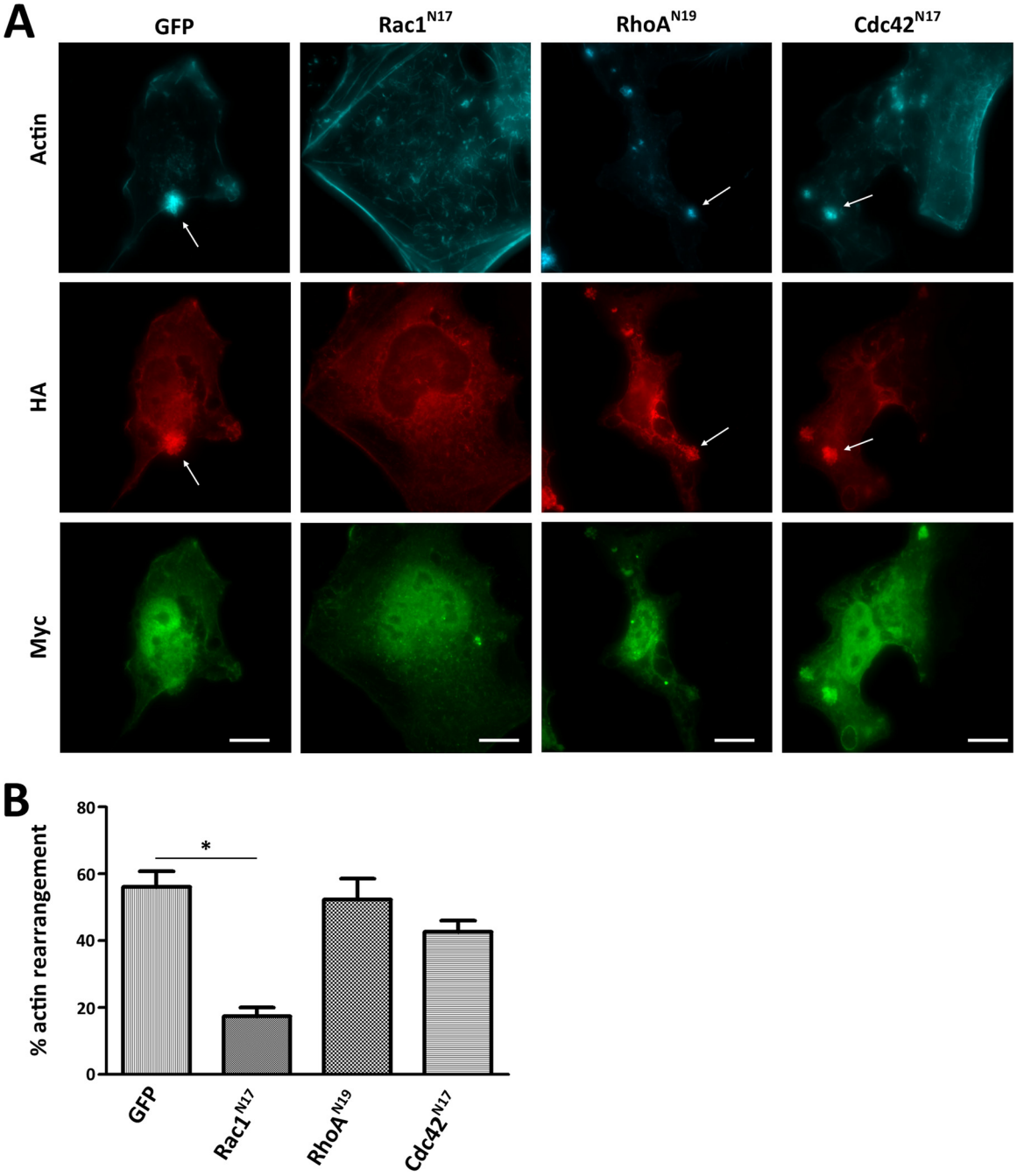


**FIG 3** EspW-induced actin reorganization is Rac1 dependent. (A) Cotransfection of HA-EspW (red) with myc-Rac1$^{N17}$ (green), but not with GFP, Myc-Cdc42$^{N17}$, and Myc-RhoA$^{N19}$, inhibited actin (blue) rearrangement (white arrow). Bar, 10 $\mu$m. (B) Quantification of cotransfected cells showing actin rearrangement. The percentage was calculated by counting 100 transfected cells (in triplicate) from three independent experiments. Results are presented as means $\pm$ SD. *, $P < 0.05$.

each of the GTPases (Rac1$^{N17}$, RhoA$^{N19}$, and Cdc42$^{N17}$). The cotransfected cells were assessed by IF for the presence of actin-rich flower-shaped structures. This revealed that inactivation of either RhoA or Cdc42 had no effect on the ability of EspW to induce actin reorganization (Fig. 3A). In contrast, inhibition of Rac1 significantly compromised the ability of EspW to induce actin rearrangements (Fig. 3A and B).

**Deletion of *espW* induces cell shrinkage that could be overcome by Rac1 activation.** To assess the role of EspW during infection, cells were infected for 3 h with wild-type (WT) EHEC, an EHEC Δ*espW* strain, or an EHEC Δ*espW* strain complemented with pEspW. Immunofluorescence reveals that infection with the EHEC Δ*espW* strain

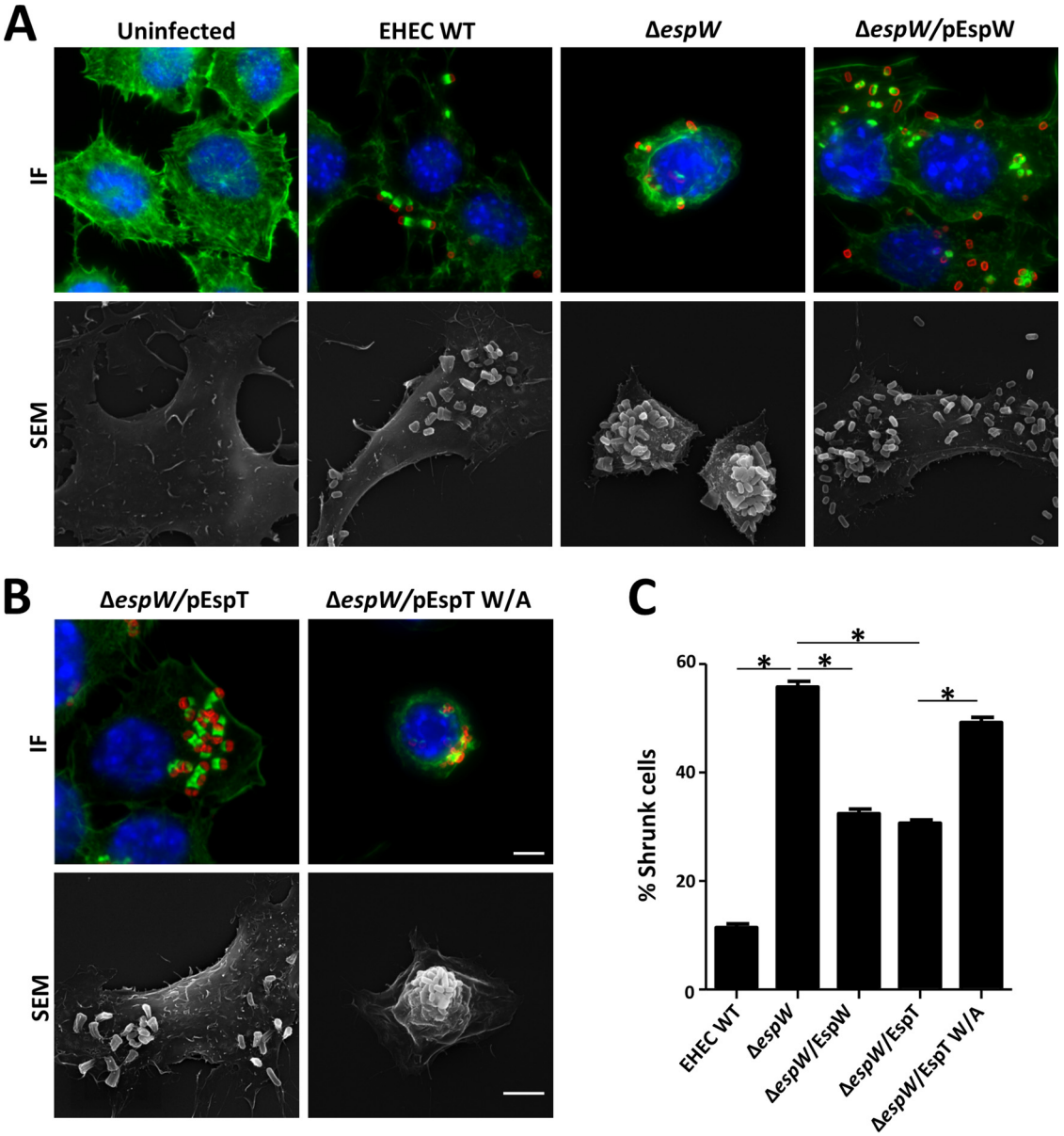


**FIG 4** EHEC Δ*espW* mutant induces cell shrinkage. (A) Shrinking of cells (visualized by IF, with actin in green and DNA in blue, and SEM) was observed following infection with an EHEC Δ*espW* strain in comparison to cells left uninfected or infected with WT EHEC (red) or an EHEC Δ*espW* strain complemented with pEspW. Bar, 5 $\mu$m. (B) Cells infected with the EHEC Δ*espW* strain expressing $EspT_{w/A}$ shrunk compared to cells infected with the EHEC Δ*espW* strain expressing WT EspT. Bar, 5 $\mu$m. (C) Quantification of phenotype observed in panel B (100 infected cells in triplicate) following infection with WT EHEC, an EHEC Δ*espW* strain, and EHEC Δ*espW* strains expressing EspW (Δ*espW*/EspW), EspT (Δ*espW*/EspT), and EspT W/A (Δ*espW*/EspT W/A). *, $P < 0.05$.

induced significant cell shrinkage (56%) compared to infection with WT EHEC (12%) (Fig. 4A). Partial complementation was observed for the cell infected with the EHEC Δ*espW* strain complemented with pEspW (32%) (Fig. 4C).

To determine if the cell shrinkage was linked with lack of activation of Rac1, cells were infected with an EHEC Δ*espW* strain overexpressing EspT, an effector known to activate Rac1 (22). The $EspT_{W/A}$ mutant, lacking the GEF activity of EspT, was used as a negative control (Fig. 4B). Expression of WT EspT significantly reduced cell shrinkage (31%) compared with cells infected with the EHEC Δ*espW* strain complemented with $pEspT_{W/A}$ (50%) (Fig. 4C).

In order to confirm that the cell shrinkage was caused by the lack of Rac1 activation, we chemically induced activation of Rac1 during infection by adding 100 nM sphin-

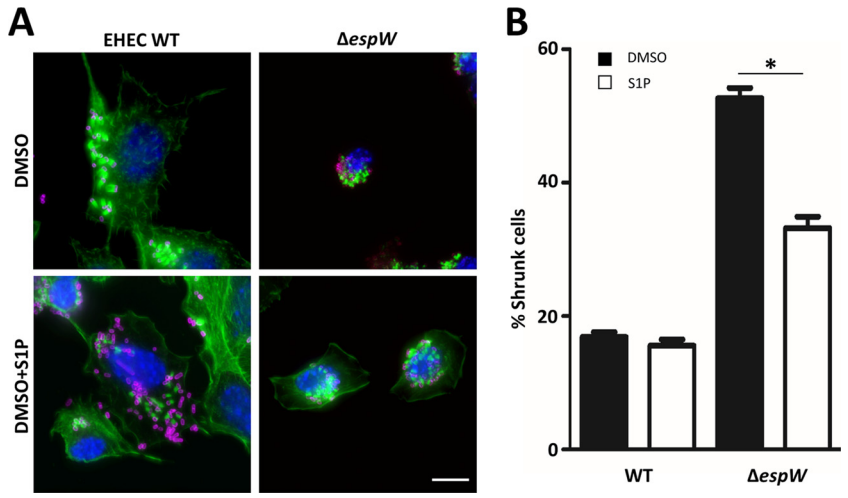


**FIG 5** Rac1 activation prevents cell shrinkage. (A) Immunofluorescence microscopy of Swiss cells (visualized with actin in green and DNA in blue) infected (magenta) with the WT or Δ*espW* EHEC strain in the presence or absence of 100 nM S1P. The presence of S1P prevented cell shrinkage. Bar, 10 $\mu$m. (B) Quantification of phenotype observed in panel B (100 cells in triplicate) infected with the WT or Δ*espW* EHEC strain in the presence (white bar) or absence (black bar) of S1P. *, $P < 0.05$.

gosine 1-phosphate (S1P) to the culture medium (28) and quantified the number of shrunken cells after infection (Fig. 5A and B). S1P treatment significantly reduced shrinking of cells infected with the EHEC Δ*espW* strain from 53% to 33% (Fig. 5B). These results suggest that EspW activates Rac-1, which stabilizes the shape of infected cells.

## DISCUSSION

In this study, we found that *espW* is common among clinical EHEC and EPEC isolates; an *espW* orthologue is also found in *Shigella boydii*. The majority of the EPEC strains contain the full-length *espW* gene, while others, mainly belonging to EPEC O55:H7, encode a truncated EspW isoform. Although the truncated form of EspW does not induce actin reorganization, it is possible that it has other biological functions.

Using a two-hybrid screen, we identified Kif15 as a specific partner of the full-length EspW isoform. Human Kif15 is a multimeric protein of 1,388 amino acids which belongs to the kinesin family (29). It has an N-terminal motor domain (residues 19 to 375) followed by a long alpha-helical rod-shaped stalk predicted to form an interrupted coiled coil. The C-terminal region has been shown to contain a putative actin interacting region (residues 743 to 1333) (30). Moreover, in HeLa cells, Kif15 has been shown to concentrate on spindle poles and microtubules in early mitosis and to localize with actin in late mitosis (31). One possibility is that Kif15 switches binding from one filament system to the other, while another possibility is that Kif15 associates with the most abundant cytoskeletal filament system (31). In this study, we mapped the EspW binding site to a segment of Kif15, amino acids 1092 to 1142. This segment is a known binding site for both Ki-67 (1017 to 1237) and actin (743 to 1333). The exact role of Kif15 during infection is still unclear, as labeling of EspW in EPEC did not allow us to localize the effector during infection. However, its recruitment to the pedestal during EPEC infection is independent of EspW. We therefore hypothesize that Kif15 recruits EspW and determines its spatial distribution, similar to the function of NHERF1 or NHERF2 toward the effector Map (32).

EPEC and EHEC, like many other enteric pathogens, target actin cytoskeleton as part of their infection strategy. The hallmark of EPEC and EHEC infection of cultured cells is formation of actin pedestal-like structures underneath the attached bacteria. In EPEC, formation of these structures is dependent on the effector Tir and activation of N-WASP and independent of activation of mammalian Rho GTPases (33). However, EspH, which is a global inhibitor of endogenous mammalian GEFs (23), is required for efficient actin

pedestal elongation (34), suggesting that Rho GTPases are partially involved in this process. Importantly, EPEC and EHEC translocate several effectors, belonging to the SopE family, which have a GEF activity toward mammalian Rho GTPases (18). *In vitro*, EspT, which activates Rac1, triggers formation of ruffles or lamelipodia, and *in vivo* it induces expression of KC and tumor necrosis factor alpha (TNF-$\alpha$) (35). In this study, we found that EspW also appears to activate Rac1, either directly or indirectly, in a compartmentalized fashion; this is in contrast to EspT, which has a more global effect. Nonetheless, the phenotype of *espW* deletion could be partially complemented by *espT*, suggesting some activity overlap. Due to poor solubility, we were not able to identify whether EspW directly activates Rac1. Importantly, multiple biological systems revealed that activation or inhibition of the Rho GTPase has to be fine-tuned both spatially and temporally. Their overactivation or inhibition have detrimental effects leading to activation of alarm signals (36) or apoptosis (37). During EPEC infection, activation of Cdc42 is limited to the bacterial binding sites (19), followed by rapid inhibition by Tir (19). The effector EspO, expressed by a selection of EPEC and EHEC strains, has been reported to inactivate EspM2 (RhoA GEF). Interestingly, deletion of *espO1* and *espO2* leads to cell shrinkage in an EspM2-dependent manner (25). Rac1 and RhoA have antagonistic effects (38). Interestingly, we found that cells infected with EHEC expressing EspM1 and EspM2 but missing EspW undergo cell shrinkage. This cell shrinkage phenotype was not associated with decreased cell attachment or with any signs of cell death, including nucleus condensation, loss of membrane permeability, or membrane blebbing, for the duration of the experiment. Interestingly, we found that EPEC and EHEC strains expressing EspM also express either EspT or EspW, suggesting that activation of RhoA and Rac1 need to be coordinated during infection. Furthermore, deletion of Rac1 impairs focal adhesion complex formation and cell spreading (39). Taken together, these observations suggest that EPEC and EHEC have developed a complex mechanism to control cell shape by manipulating the localization and activation of RhoA and Rac1. Any dysregulation leading to an uncontrolled activation leads to dramatic cell morphology changes. Further studies will be needed in order to understand the spatiotemporal regulation of the Rho GTPase during EPEC and EHEC infections.

## MATERIALS AND METHODS

**Bacterial strains, growth conditions, and cell culture.** The bacterial strains used in this study and their origins are listed in Table 2. Bacteria were grown from a single colony in Luria-Bertani (LB) broth in a shaking incubator (200 rpm) at 37°C for 18 h or on agar supplemented with ampicillin (100 $\mu$g/ml) or kanamycin (50 $\mu$g/ml). For cell infections, EHEC strains were grown in LB in a shaking incubator (200 rpm) at 37°C for 8 h and then subcultured (1/500) in Dulbecco's modified Eagle's medium (DMEM) with low glucose and grown overnight at 37°C without agitation in a 5% $CO_2$ incubator (primed culture).

*Saccharomyces cerevisiae* (AH109) was grown in YPDA medium (20 g/liter Difco peptone, 10 g/liter yeast extract, 2% glucose, and 0.003% adenine hemisulfate) for 48 h at 30°C. For the yeast two-hybrid screen, clones containing interaction partners were selected on high-stringency quadruple-dropout (QDO) medium lacking leucine, tryptophan, histidine, and adenine in the presence of X-$\alpha$-Gal (Clontech Laboratories, Inc.). Successful transformation with bait and prey plasmids was selected by plating on double-dropout (DDO) medium lacking leucine and tryptophan. Bait-prey interactions were assessed by streaking the transformed clones from DDO onto QDO selection medium.

Swiss 3T3 and HeLa cells were maintained in DMEM with 4,500 mg/ml glucose (Sigma) or DMEM with 1,000 mg/ml glucose (Sigma), respectively, supplemented with 10% (vol/vol) heat-inactivated fetal calf serum (FCS; Gibco), 4 mM GlutaMAX (Gibco), and 0.1 mM nonessential amino acids at 37°C in 5% $CO_2$.

**Plasmids and molecular techniques.** Plasmids used in this study are listed in Table 2, and primers are listed in Table S1 in the supplemental material.

The EHEC Δ*espW* (ICC1111) strain was generated using a lambda red-based mutagenesis system (40) in which *espW* was replaced by a kanamycin cassette. Plasmid pSB315 was the source of the kanamycin resistance gene (*aphT*), which was purified following EcoRI restriction digestion. Primer pair P23/P24 was used to PCR amplify *espW* with 500-bp upstream and downstream flanking regions from *E. coli* O157:H7 (85-170) genomic DNA. The PCR product was cloned into TOPO Blunt II vector (Invitrogen), and *espW* was removed by inverse PCR using the primer pair P25/P26. The linear PCR product was then EcoRI digested to allow ligation of the kanamycin cassette. The insert was then amplified using the primer pair P23/P24 and the PCR product electroporated into WT EHEC containing pKD46 encoding the lambda red recombinase. Transformants were selected on kanamycin plates, and the deletion of *espW* was confirmed by PCR and DNA sequencing (using primer pair P27/P28).

*espW* and $espW_{1-206}$ were cloned into the bacterial expression vector pRK5-HA following amplification from 85-170 genomic DNA using primer pairs P1/P2 and P1/P3, generating plasmids pICC1727 and

**TABLE 2** List of strains and plasmids

| Strain or plasmid | Description/function | Source/reference |
|---|---|---|
| Strains | | |
| 85-170 | EHEC O157:H7, *stx* mutant | 44 |
| ICC1111 | 85-170 Δ*espW* | This study |
| AH109 | *S. cerevisiae* MAT$\alpha$ mating type with ADE2, HIS3, MEL1, and LacZ reporters for interaction and TRP1 and LEU2 selection markers | Clontech |
| Y187 | *S. cerevisiae* MAT$\alpha$ mating type with MEL1 and LacZ reporters and TRP1 and LEU2 selection markers | Clontech |
| Plasmids | | |
| pRK5-HA (Amp$^r$) | Eukaryotic expression vector of HA-tagged protein | 45 |
| pICC1396 | pRK5 expressing HA-tagged mCherry | This study |
| pICC1727 | pRK5 expressing HA-tagged EspW | This study |
| pICC1728 | pRK5 expressing HA-tagged EspW$_{1–206}$ | This study |
| pRK5-myc (Amp$^r$) | Eukaryotic expression vector of myc-tagged protein | Clontech |
| pICC563 | pRK5 expressing myc-tagged GFP | 46 |
| pRK5-myc-Rac1$^{N17}$ | pRK5 expressing myc-tagged Rac1$^{N17}$ | 47 |
| pRK5-myc-RhoA$^{N19}$ | pRK5 expressing myc-tagged RhoA$^{N19}$ | 47 |
| pRK5-myc-Cdc42$^{N17}$ | pRK5 expressing myc-tagged Cdc42$^{N17}$ | 47 |
| pICC1914 | pRK5 expressing myc-tagged Kif15$_{1092–1368}$ | This study |
| pSA10 (Amp$^r$) | pKK177-3 derivative containing *lac*$^I$ | 42 |
| pICC1732 | pSA10 derivative expressing EspW | This study |
| pICC461 | pSA10 derivative expressing EspT | 22 |
| pICC1205 | pSA10 derivative expressing EspT$_{W/A}$ | 22 |
| pKD46 (Amp$^r$) | Coding for the lambda red recombinase | 40 |
| pSB315 (Kan$^r$) | Coding for the kanamycin resistance *aphT* cassette | 48 |
| TOPO Blunt II (Kan$^r$) | TOPO cloning of blunt PCR products | Invitrogen |
| pGBT9 | Gal4 DNA binding domain, selective for −Trp medium expression for proteins in yeast | Clontech |
| pICC1714 | pGBT9 derivative expressing EspW | This study |
| pICC1715 | pGBT9 derivative expressing EspW$_{1–206}$ | This study |
| pGAD-T7-AD | Yeast two-hybrid prey expression vector | Clontech |
| pICC1723 | pGAD derivative expressing Kif15$_{1092–1368}$ | This study |
| pICC1724 | pGAD derivative expressing Kif15$_{1142–1347}$ | This study |
| pICC1725 | pGAD derivative expressing Kif15$_{1092–1347}$ | This study |
| pICC1726 | pGAD derivative expressing Kif15$_{1142–1368}$ | This study |
| pICC1752 | pGAD derivative expressing Kif15$_{1092–1142}$ | This study |

pICC1728. *mCherry* was amplified from pmcherry-miniSOG-C1 (41) using primers P4/P5, generating plasmid pICC1396. Plasmid pICC1727 was used as the template to amplify *espW* (P10/P11) and further cloned into pSA10 (42), generating plasmid pICC1732.

*espW* and *espW*$_{1–206}$ were amplified using primers P10/P12 with plasmids pICC1727 and pICC1728, respectively, and were cloned into the EcoRI/BamHI restriction sites of pGBT9 (Clontech), generating plasmids pICC1714 and pICC1715. Kif15$_{1092–1368}$ was identified as a binding partner for EspW by a yeast two-hybrid screen (Clontech). *kif15*$_{1092–1368}$ was amplified by PCR with primers P13/P14 and cloned into pGAD-T7-AD (Clontech) using NdeI/XhoI as restriction sites, generating plasmid pICC1723. We used plasmid pICC1723 as a template to amplify *kif15*$_{1142–1347}$, *kif15*$_{1092–1347}$, and *kif15*$_{1142–1368}$ with primers P15/P16, P17/P16, and P15/P18, respectively. The genes were cloned into pGAD-T7 using NdeI/XhoI restriction sites, generating plasmids pICC1724, pICC1725, and pICC1726. Plasmid pICC1752, containing *kif15*$_{1092–1142}$, was generated by inverse PCR using plasmid pICC1723 as the template and phosphorylated primers P19/P20. *kif15*$_{1092–1368}$ was cloned into the EcoRI/HindIII sites of the bacterial protein expression vector pRK5-Myc (Clontech) following amplification using primer pair P21/P22 and plasmid pICC1723 as a template, generating plasmid pICC1914. EPEC clinical isolates were screened first for the presence of *espW* by PCR using primer pair P29/P30. We further screened all of the *espW*-negative strains for the presence of *espW*$_{1–206}$ using primer pair P31/P32.

**Yeast two-hybrid assays.** Yeast two-hybrid screening using EspW as prey and a cDNA library as bait was performed as described previously (43). Briefly, a pretransformed MATCHMAKER HeLa cell cDNA library (Clontech) was screened according to the manufacturer's protocol for proteins interacting with EspW. The lithium acetate method was used to transform pGBT9-espW (pICC1714) (Table 2) into yeast strain AH109 (MAT**a**), and transformants were selected on Trp-minus-synthetic-defined agar plates. Following mating with the Y187 (MAT$\alpha$) yeast strain containing the cDNA library, diploids cells were selected on DDO and QDO media for selection of protein interactions. The cDNA-containing pGADT7 plasmid was rescued from positive clones and the cDNA identified by DNA sequencing. The prey plasmid and derivatives (Table 2) were then retransformed into AH109 either on its own to determine possible self-activation or with pICC1714 or pICC1715 to confirm interaction by direct yeast two-hybrid assay.

**Infection of Swiss 3T3 and HeLa cells.** Forty-eight hours prior to infection, Swiss 3T3 or HeLa cells were seeded in 24-well plates containing 13-mm glass coverslips (VWR International) at a density of $5 \times 10^5$ cells per well. Before infection, the cells were washed 3 times with phosphate-buffered saline (PBS) and the medium was replaced with fresh DMEM without FCS. Cells in 24-well plates were infected with 20 $\mu$l of primed cultures. The plates were then centrifuged at 200 rpm for 5 min at room temperature, and infections were carried out for 3 h at 37°C in 5% $CO_2$ without agitation. After infection, monolayers were washed at least 10 times in PBS to remove the bacteria and were fixed for immunofluorescence (to assess cell morphology) as described below.

For sphingosine 1-phosphate (S1P) (Sigma-Aldrich) treatment, S1P was dissolved in dimethyl sulfoxide (DMSO) (Sigma-Aldrich) and added to DMEM to attain a final concentration of 100 nM.

**Transfection.** Swiss 3T3 and HeLa cells were transfected for 24 h using Lipofectamine 2000 (Invitrogen) and GeneJuice (Merck Millipore), respectively, according to the manufacturer's instructions.

**Immunofluorescence and microscopy.** Coverslips were fixed with 3% paraformaldehyde (PFA) for 15 min before washing 3 more times with PBS. Cells were quenched for 10 min with 50 mM $NH_4Cl$, permeabilized for 4 min in PBS–0.2% Triton X-100, and washed 3 times in PBS. The coverslips were blocked for 15 min in 0.2% bovine serum albumin (BSA)–PBS before incubation with primary and secondary antibodies. The primary antibodies mouse anti-hemagglutinin (HA) (Cambridge Bioscience), chicken anti-Myc (Millipore), and rabbit polyclonal anti-O157 (Roberto la Ragione, Veterinary Laboratory Agency, United Kingdom) were used at a dilution of 1:500. Coverslips were incubated with the primary antibody for 1 h, washed 3 times in PBS, and incubated with the secondary antibodies. AMCA-, Cy2-, RRX-, or Cy5-conjugated donkey anti-mouse, anti-chicken, and anti-rabbit antibodies (Jackson ImmunoResearch) were used as secondary antibodies. All dilutions were in PBS–0.2% BSA. Actin was detected with tetramethyl rhodamine isothiocyanate (TRITC)-conjugated phalloidin (1:500 dilution) (Sigma), phalloidin Alexa Fluor 350, or phalloidin Oregon green 488 (1:100 dilution) (Invitrogen). DNA was stained with 4′,6-diamidino-2-phenylindole (DAPI) (1:1,000 dilution). Coverslips were mounted on slides using ProLong Gold antifade reagent (Invitrogen) and examined by conventional epifluorescence microscopy using a Zeiss Axio LSM-510 microscope. Images were deconvoluted, processed using Axio Vision 4.8 LE software (Zeiss), and trimmed using Adobe Photoshop CS4.

**SEM.** For scanning electron microscopy (SEM), cells were washed 3 times in phosphate buffer, pH 7.4, and then fixed with 2.5% glutaraldehyde in phosphate buffer, pH 7.4. Cells were washed 3 times in phosphate buffer before being postfixed in 1% osmium tetroxide for 1 h. Cells were then washed 3 times in phosphate buffer and dehydrated for 15 min in graded ethanol solutions from 50% to 100%. The cells were then transferred to an Emitech K850 critical point drier and processed according to the manufacturer's instructions. The coverslips were coated in gold/palladium mix using an Emitech Sc762 mini sputter. Samples for SEM were then examined blindly at an accelerating voltage of 25 kV using a JEOL JSM-6390.

**Statistical analysis.** All data were analyzed with GraphPad Prism software, using one-way analysis of variance (ANOVA). Results were expressed as means and standard deviations (SD). Statistical significance was determined by a two-tailed Student *t* test. A *P* value of $<0.05$ was considered significant.

## SUPPLEMENTAL MATERIAL

Supplemental material for this article may be found at https://doi.org/10.1128/IAI.00244-17.

**SUPPLEMENTAL FILE 1,** PDF file, 1.1 MB.

## ACKNOWLEDGMENTS

This work was supported by grants from The Wellcome Trust, the BBSRC, and MRC.

## REFERENCES

1. Chen HD, Frankel G. 2005. Enteropathogenic *Escherichia coli*: unravelling pathogenesis. FEMS Microbiol Rev 29:83–98. https://doi.org/10.1016/j.femsre.2004.07.002.
2. Collins JW, Keeney KM, Crepin VF, Rathinam VA, Fitzgerald KA, Finlay BB, Frankel G. 2014. *Citrobacter rodentium*: infection, inflammation and the microbiota. Nat Rev Microbiol 12:612–623. https://doi.org/10.1038/nrmicro3315.
3. Knutton S, Lloyd DR, McNeish AS. 1987. Adhesion of enteropathogenic *Escherichia coli* to human intestinal enterocytes and cultured human intestinal mucosa. Infect Immun 55:69–77.
4. Knutton S, Rosenshine I, Pallen MJ, Nisan I, Neves BC, Bain C, Wolff C, Dougan G, Frankel G. 1998. A novel EspA-associated surface organelle of enteropathogenic *Escherichia coli* involved in protein translocation into epithelial cells. EMBO J 17:2166–2176. https://doi.org/10.1093/emboj/17.8.2166.
5. McDaniel TK, Jarvis KG, Donnenberg MS, Kaper JB. 1995. A genetic locus of enterocyte effacement conserved among diverse enterobacterial pathogens. Proc Natl Acad Sci U S A 92:1664–1668. https://doi.org/10.1073/pnas.92.5.1664.
6. Wong AR, Pearson JS, Bright MD, Munera D, Robinson KS, Lee SF, Frankel G, Hartland EL. 2011. Enteropathogenic and enterohaemorrhagic *Escherichia coli:* even more subversive elements. Mol Microbiol 80:1420–1438. https://doi.org/10.1111/j.1365-2958.2011.07661.x.
7. Crepin VF, Girard F, Schuller S, Phillips AD, Mousnier A, Frankel G. 2010. Dissecting the role of the Tir:Nck and Tir:IRTKS/IRSp53 signalling pathways in vivo. Mol Microbiol 75:308–323. https://doi.org/10.1111/j.1365-2958.2009.06938.x.
8. Kenny B, Finlay BB. 1997. Intimin-dependent binding of enteropathogenic *Escherichia coli* to host cells triggers novel signaling events, including tyrosine phosphorylation of phospholipase C-gamma1. Infect Immun 65:2528–2536.
9. Vingadassalom D, Kazlauskas A, Skehan B, Cheng HC, Magoun L, Robbins D, Rosen MK, Saksela K, Leong JM. 2009. Insulin receptor tyrosine kinase substrate links the *E. coli* O157:H7 actin assembly effectors Tir and

EspF(U) during pedestal formation. Proc Natl Acad Sci U S A 106:6754–6759. https://doi.org/10.1073/pnas.0809131106.
10. Weiss SM, Ladwein M, Schmidt D, Ehinger J, Lommel S, Stading K, Beutling U, Disanza A, Frank R, Jansch L, Scita G, Gunzer F, Rottner K, Stradal TE. 2009. IRSp53 links the enterohemorrhagic *E. coli* effectors Tir and EspFU for actin pedestal formation. Cell Host Microbe 5:244–258. https://doi.org/10.1016/j.chom.2009.02.003.
11. Campellone KG, Robbins D, Leong JM. 2004. EspFU is a translocated EHEC effector that interacts with Tir and N-WASP and promotes Nck-independent actin assembly. Dev Cell 7:217–228. https://doi.org/10.1016/j.devcel.2004.07.004.
12. Garmendia J, Phillips AD, Carlier MF, Chong Y, Schuller S, Marches O, Dahan S, Oswald E, Shaw RK, Knutton S, Frankel G. 2004. TccP is an enterohaemorrhagic *Escherichia coli* O157:H7 type III effector protein that couples Tir to the actin-cytoskeleton. Cell Microbiol 6:1167–1183. https://doi.org/10.1111/j.1462-5822.2004.00459.x.
13. Caron E, Crepin VF, Simpson N, Knutton S, Garmendia J, Frankel G. 2006. Subversion of actin dynamics by EPEC and EHEC. Curr Opin Microbiol 9:40–45. https://doi.org/10.1016/j.mib.2005.12.008.
14. Millard TH, Sharp SJ, Machesky LM. 2004. Signalling to actin assembly via the WASP (Wiskott-Aldrich syndrome protein)-family proteins and the Arp2/3 complex. Biochem J 380:1–17. https://doi.org/10.1042/bj20040176.
15. Heasman SJ, Ridley AJ. 2008. Mammalian Rho GTPases: new insights into their functions from in vivo studies. Nat Rev Mol Cell Biol 9:690–701. https://doi.org/10.1038/nrm2476.
16. Hall A. 1998. Rho GTPases and the actin cytoskeleton. Science 279:509–514. https://doi.org/10.1126/science.279.5350.509.
17. Nayak RC, Chang KH, Vaitinadin NS, Cancelas JA. 2013. Rho GTPases control specific cytoskeleton-dependent functions of hematopoietic stem cells. Immunol Rev 256:255–268. https://doi.org/10.1111/imr.12119.
18. Bulgin R, Raymond B, Garnett JA, Frankel G, Crepin VF, Berger CN, Arbeloa A. 2010. Bacterial guanine nucleotide exchange factors SopE-like and WxxxE effectors. Infect Immun 78:1417–1425. https://doi.org/10.1128/IAI.01250-09.
19. Berger CN, Crepin VF, Jepson MA, Arbeloa A, Frankel G. 2009. The mechanisms used by enteropathogenic *Escherichia coli* to control filopodia dynamics. Cell Microbiol 11:309–322. https://doi.org/10.1111/j.1462-5822.2008.01254.x.
20. Jepson MA, Pellegrin S, Peto L, Banbury DN, Leard AD, Mellor H, Kenny B. 2003. Synergistic roles for the Map and Tir effector molecules in mediating uptake of enteropathogenic *Escherichia coli* (EPEC) into nonphagocytic cells. Cell Microbiol 5:773–783. https://doi.org/10.1046/j.1462-5822.2003.00315.x.
21. Arbeloa A, Bulgin RR, MacKenzie G, Shaw RK, Pallen MJ, Crepin VF, Berger CN, Frankel G. 2008. Subversion of actin dynamics by EspM effectors of attaching and effacing bacterial pathogens. Cell Microbiol 10:1429–1441. https://doi.org/10.1111/j.1462-5822.2008.01136.x.
22. Bulgin RR, Arbeloa A, Chung JC, Frankel G. 2009. EspT triggers formation of lamellipodia and membrane ruffles through activation of Rac-1 and Cdc42. Cell Microbiol 11:217–229. https://doi.org/10.1111/j.1462-5822.2008.01248.x.
23. Dong N, Liu L, Shao F. 2010. A bacterial effector targets host DH-PH domain RhoGEFs and antagonizes macrophage phagocytosis. EMBO J 29:1363–1376. https://doi.org/10.1038/emboj.2010.33.
24. Kenny B, Ellis S, Leard AD, Warawa J, Mellor H, Jepson MA. 2002. Co-ordinate regulation of distinct host cell signalling pathways by multifunctional enteropathogenic *Escherichia coli* effector molecules. Mol Microbiol 44:1095–1107. https://doi.org/10.1046/j.1365-2958.2002.02952.x.
25. Morita-Ishihara T, Miura M, Iyoda S, Izumiya H, Watanabe H, Ohnishi M, Terajima J. 2013. EspO1-2 regulates EspM2-mediated RhoA activity to stabilize formation of focal adhesions in enterohemorrhagic *Escherichia coli*-infected host cells. PLoS One 8:e55960. https://doi.org/10.1371/journal.pone.0055960.
26. Tobe T, Beatson SA, Taniguchi H, Abe H, Bailey CM, Fivian A, Younis R, Matthews S, Marches O, Frankel G, Hayashi T, Pallen MJ. 2006. An extensive repertoire of type III secretion effectors in *Escherichia coli* O157 and the role of lambdoid phages in their dissemination. Proc Natl Acad Sci U S A 103:14941–14946. https://doi.org/10.1073/pnas.0604891103.
27. Wick LM, Qi W, Lacher DW, Whittam TS. 2005. Evolution of genomic content in the stepwise emergence of *Escherichia coli* O157:H7. J Bacteriol 187:1783–1791. https://doi.org/10.1128/JB.187.5.1783-1791.2005.
28. Gonzalez E, Kou R, Michel T. 2006. Rac1 modulates sphingosine 1-phosphate-mediated activation of phosphoinositide 3-kinase/Akt signaling pathways in vascular endothelial cells. J Biol Chem 281:3210–3216. https://doi.org/10.1074/jbc.M510434200.
29. Drechsler H, McHugh T, Singleton MR, Carter NJ, McAinsh AD. 2014. The kinesin-12 Kif15 is a processive track-switching tetramer. eLife 3:e01724.
30. Klejnot M, Falnikar A, Ulaganathan V, Cross RA, Baas PW, Kozielski F. 2014. The crystal structure and biochemical characterization of Kif15: a bifunctional molecular motor involved in bipolar spindle formation and neuronal development. Acta Crystallogr D Biol Crystallogr 70:123–133. https://doi.org/10.1107/S1399004713028721.
31. Buster DW, Baird DH, Yu W, Solowska JM, Chauviere M, Mazurek A, Kress M, Baas PW. 2003. Expression of the mitotic kinesin Kif15 in postmitotic neurons: implications for neuronal migration and development. J Neurocytol 32:79–96. https://doi.org/10.1023/A:1027332432740.
32. Martinez E, Schroeder GN, Berger CN, Lee SF, Robinson KS, Badea L, Simpson N, Hall RA, Hartland EL, Crepin VF, Frankel G. 2010. Binding to Na(+)/H(+) exchanger regulatory factor 2 (NHERF2) affects trafficking and function of the enteropathogenic *Escherichia coli* type III secretion system effectors Map, EspI and NleH. Cell Microbiol 12:1718–1731. https://doi.org/10.1111/j.1462-5822.2010.01503.x.
33. Ben-Ami G, Ozeri V, Hanski E, Hofmann F, Aktories K, Hahn KM, Bokoch GM, Rosenshine I. 1998. Agents that inhibit Rho, Rac, and Cdc42 do not block formation of actin pedestals in HeLa cells infected with enteropathogenic *Escherichia coli*. Infect Immun 66:1755–1758.
34. Tu X, Nisan I, Yona C, Hanski E, Rosenshine I. 2003. EspH, a new cytoskeleton-modulating effector of enterohaemorrhagic and enteropathogenic *Escherichia coli*. Mol Microbiol 47:595–606. https://doi.org/10.1046/j.1365-2958.2003.03329.x.
35. Raymond B, Crepin VF, Collins JW, Frankel G. 2011. The WxxxE effector EspT triggers expression of immune mediators in an Erk/JNK and NF-kappaB-dependent manner. Cell Microbiol 13:1881–1893. https://doi.org/10.1111/j.1462-5822.2011.01666.x.
36. Keestra AM, Winter MG, Auburger JJ, Frassle SP, Xavier MN, Winter SE, Kim A, Poon V, Ravesloot MM, Waldenmaier JF, Tsolis RM, Eigenheer RA, Baumler AJ. 2013. Manipulation of small Rho GTPases is a pathogen-induced process detected by NOD1. Nature 496:233–237. https://doi.org/10.1038/nature12025.
37. Fiorentini C, Falzano L, Travaglione S, Fabbri A. 2003. Hijacking Rho GTPases by protein toxins and apoptosis: molecular strategies of pathogenic bacteria. Cell Death Differ 10:147–152. https://doi.org/10.1038/sj.cdd.4401151.
38. Chauhan BK, Lou M, Zheng Y, Lang RA. 2011. Balanced Rac1 and RhoA activities regulate cell shape and drive invagination morphogenesis in epithelia. Proc Natl Acad Sci U S A 108:18289–18294. https://doi.org/10.1073/pnas.1108993108.
39. Guo F, Debidda M, Yang L, Williams DA, Zheng Y. 2006. Genetic deletion of Rac1 GTPase reveals its critical role in actin stress fiber formation and focal adhesion complex assembly. J Biol Chem 281:18652–18659. https://doi.org/10.1074/jbc.M603508200.
40. Datsenko KA, Wanner BL. 2000. One-step inactivation of chromosomal genes in *Escherichia coli* K-12 using PCR products. Proc Natl Acad Sci U S A 97:6640–6645. https://doi.org/10.1073/pnas.120163297.
41. Shu X, Lev-Ram V, Deerinck TJ, Qi Y, Ramko EB, Davidson MW, Jin Y, Ellisman MH, Tsien RY. 2011. A genetically encoded tag for correlated light and electron microscopy of intact cells, tissues, and organisms. PLoS Biol 9:e1001041. https://doi.org/10.1371/journal.pbio.1001041.
42. Schlosser-Silverman E, Elgrably-Weiss M, Rosenshine I, Kohen R, Altuvia S. 2000. Characterization of *Escherichia coli* DNA lesions generated within J774 macrophages. J Bacteriol 182:5225–5230. https://doi.org/10.1128/JB.182.18.5225-5230.2000.
43. Simpson N, Shaw R, Crepin VF, Mundy R, FitzGerald AJ, Cummings N, Straatman-Iwanowska A, Connerton I, Knutton S, Frankel G. 2006. The enteropathogenic *Escherichia coli* type III secretion system effector Map binds EBP50/NHERF1: implication for cell signalling and diarrhoea. Mol Microbiol 60:349–363. https://doi.org/10.1111/j.1365-2958.2006.05109.x.
44. Tzipori S, Karch H, Wachsmuth KI, Robins-Browne RM, O'Brien AD, Lior H, Cohen ML, Smithers J, Levine MM. 1987. Role of a 60-megadalton plasmid and Shiga-like toxins in the pathogenesis of infection caused by enterohemorrhagic *Escherichia coli* O157:H7 in gnotobiotic piglets. Infect Immun 55:3117–3125.
45. Dolezal P, Aili M, Tong J, Jiang JH, Marobbio CM, Lee SF, Schuelein R, Belluzzo S, Binova E, Mousnier A, Frankel G, Giannuzzi G, Palmieri F, Gabriel K, Naderer T, Hartland EL, Lithgow T. 2012. *Legionella pneumo-*

*phila* secretes a mitochondrial carrier protein during infection. PLoS Pathog 8:e1002459. https://doi.org/10.1371/journal.ppat.1002459.
46. Clements A, Smollett K, Lee SF, Hartland EL, Lowe M, Frankel G. 2011. EspG of enteropathogenic and enterohemorrhagic *E. coli* binds the Golgi matrix protein GM130 and disrupts the Golgi structure and function. Cell Microbiol 13:1429–1439. https://doi.org/10.1111/j.1462-5822.2011.01631.x.
47. Li X, Saint-Cyr-Proulx E, Aktories K, Lamarche-Vane N. 2002. Rac1 and Cdc42 but not RhoA or Rho kinase activities are required for neurite outgrowth induced by the Netrin-1 receptor DCC (deleted in colorectal cancer) in N1E-115 neuroblastoma cells. J Biol Chem 277:15207–15214. https://doi.org/10.1074/jbc.M109913200.
48. Galan JE, Ginocchio C, Costeas P. 1992. Molecular and functional characterization of the *Salmonella* invasion gene invA: homology of InvA to members of a new protein family. J Bacteriol 174:4338–4349. https://doi.org/10.1128/jb.174.13.4338-4349.1992.